# Dual cation- and anion-based redox process in lithium titanium oxysulfide thin film cathodes

Vincent Dubois, Brigitte Pecquenard, Samantha Soulé, Hervé Martinez, Frédéric Le Cras

ACS APPLIED MATERIALS & INTERFACES



Article

# Dual cation- and anion-based redox process in lithium titanium oxysulfide thin film cathodes for all-solid-state lithium-ion batteries

Vincent Dubois, Brigitte Pecquenard, Samantha Soulé, Herve Martinez, and Frédéric Le Cras

*ACS Appl. Mater. Interfaces*, **Just Accepted Manuscript** • DOI: 10.1021/acsami.6b11987 • Publication Date (Web): 21 Dec 2016



ACS Publications

ACS Applied Materials & Interfaces is published by the American Chemical Society.
1155 Sixteenth Street N.W., Washington, DC 20036

# Dual Cation- and Anion-Based Redox Process in Lithium Titanium Oxysulfide Thin Film Cathodes for All-Solid-State Lithium-Ion Batteries

Vincent Dubois[a,b], Brigitte Pecquenard*[a], Samantha Soulé[c], Hervé Martinez[c], and Frédéric Le Cras*[d,e]

[a]*CNRS, Université de Bordeaux, ICMCB UPR 9048 and Bordeaux INP, F-33600 Pessac, France.*

[b]*ST Microelectronics, 16 rue Pierre et Marie Curie, F-37071 Tours, France*

[c]*IPREM-ECP CNRS UMR 5234, Université de Pau, 2 avenue Pierre Angot, F-64053 Pau, France*

[d]*CEA LETI, Minatec Campus, 17 rue des Martyrs, F-38054 Grenoble, France.*

[e]*Université Grenoble Alpes, F-38000 Grenoble, France*

*Corresponding authors: *frederic.lecras@cea.fr* , *brigitte.pecquenard@icmcb.cnrs.fr*

**Abstract:** A dual redox process involving $Ti^{3+}/Ti^{4+}$ cation species and $S^{2-}/(S_2)^{2-}$ anion species is highlighted in oxygenated lithium titanium sulfide thin film electrodes during lithium (de)insertion, leading to a high specific capacity. These cathodes for all-solid-state lithium-ion microbatteries are synthesized by sputtering of $LiTiS_2$ targets prepared by different means. The limited oxygenation of the films that is induced during the sputtering process favors the occurrence of the $S^{2-}/(S_2)^{2-}$ redox process at the expense of the $Ti^{3+}/Ti^{4+}$ one during the battery operation, and influences its voltage profile. Finally, a perfect reversibility of both electrochemical processes is observed, whatever the initial film composition. All-solid-state lithium microbatteries using these amorphous lithiated titanium disulfide thin films and operated between 1.5-3.0 $V/Li^+/Li$ deliver a greater capacity (210-270 mAh $g^{-1}$) than $LiCoO_2$, with a perfect capacity retention (-0.0015 % $cycle^{-1}$).

**Keywords:** $LiTiS_2$, thin films, all-solid-state lithium batteries, titanium sulfide, disulfide pairs

## 1. Introduction

The development of self-powered nomadic, wearable or implantable miniaturized electronics devices, boosted by the growing interest for the Internet of things (IoT), is made possible by the progress in the development of highly integrated and low power consumption components (MEMS, CMOS, transmitters), but is finally often faced with the lack of suitable energy storage solutions. Indeed, these new applications demand particular features for the embedded power source in terms of thickness, footprint, flexibility, safety, capacity and voltage, which cannot be fulfilled in particular by conventional batteries. Optimized solutions for part of these needs should be found among thin film batteries (primary or secondary) based on different chemistries (Zn/Polyaniline, Zn/$MnO_2$, Li/$LiCoO_2$,…) or obtained by different manufacturing processes (ink-jet printing, screen printing, tape casting, sputtering,…).[1,2] All-solid-state thin film batteries, manufactured by sequential deposition of thin films using vacuum deposition techniques such as sputtering, are particularly attractive when a reduced footprint, a very low thickness, a thermal and mechanical resistance and/or a high integration with microelectronic components is required. In this context, all-solid-state thin film batteries, also called microbatteries, are becoming emerging power sources in the microelectronics industry nearly 30 years after the achievement of the first proofs of concept.[3-9]

Contrary to bulk-type lithium batteries, metallic lithium is usually used as the negative electrode in all-solid-state lithium microbatteries, since the solid glassy electrolyte (typically LiPON) is able to prevent the formation of lithium dendrites during the charge.[10] Nevertheless, the deposition of lithium thin films at the industrial scale is actually a real issue. In addition, the presence of metallic lithium in the cells limits their thermal resistance, making them for instance incompatible with the reflow soldering process used to connect the electronic component on the printed circuit board. Therefore, lithium-ion or 'lithium-free' cell designs,[11,12] and consequently lithiated materials at the positive electrode, are preferably envisaged for microbatteries with improved performance. In this context, the aim of this study was to develop a new lithiated positive electrode material with possible

advantages over the widespread $LiCoO_2$ cathode material.[13-17] The latter comprise in particular a lower operating voltage (~ 2V) more adapted to energy harvesting components and low power consumption CMOS circuits, the absence of a compulsory post-deposition annealing and a slightly higher volumetric capacity (≥ 67 $\mu Ah.cm^{-2}$ $\mu m^{-1}$). Previous work achieved on thin film cathodes synthesized by sputtering of a titanium sulfide ($TiS_2$) target has already highlighted that insertion/de-insertion of lithium in the resulting amorphous materials is highly reversible in the voltage range [1-3 $V/Li^+/Li$] and lead to a high volumetric capacity.[18] This work is therefore devoted to the synthesis of lithiated titanium disulfide thin films electrodes (theoretical capacity: 225 mAh $g^{-1}$, 68 $\mu Ah\ cm^{-2}$ $\mu m^{-1}$) prepared by sputtering of a $LiTiS_2$ target, then to their physico-chemical characterization, and to the investigation of their electrochemical behavior in all-solid-state lithium microbatteries.

## 2. Experimental Section

*Preparation of sputtering targets*: $LiTiS_2$ sputtering targets were synthesized by three different ways. The first route (referred as R1) consisted in the chemical intercalation of lithium into $TiS_2$ using a n-butyl lithium reagent.[19] This preparation was performed at room temperature in an argon-filled glovebox containing less than 1 ppm $H_2O$. A solution of 1.6 M n-butyl lithium in anhydrous hexane was added dropwise into a vessel containing dry hexane and dispersed $TiS_2$ powder (Aldrich, 99.9 %), so that a 50% excess of n butyl-lithium at a concentration of 0.2 M was reached at the end. Then, the suspension remained stirred during one week. The resulting fine powder was then filtered, rinsed using anhydrous hexane and dried under vacuum at 100°C. About 8 g of $LiTiS_2$ were prepared at a time. Solid state reaction of a mixture of $TiS_2$ (Aldrich, 99.9%, 1 µm), Ti powder (Alfa Aesar, 99.9%, 150 mesh) and $Li_2S$ (Alfa Aesar, 99.9%) with a molar ratio 3:1:2 was used as an alternative route (referred as R2) and allowed the preparation of larger batches of $LiTiS_2$.[20] Precursors were ground together using a planetary ball-mill and an argon-filled agate jar, prior being annealed under argon. All material transfers were carried out without any air exposure. Both sputtering targets (50

mm diameter, ~ 3 mm thick) were prepared from about 15 g of $LiTiS_2$ powder prepared either by chemical reaction or solid state reaction. Targets were obtained by cold pressing at 60 MPa in a cylindrical stainless steel die inside the glove box. The one from $LiTiS_2$ precursor prepared by solid state reaction was further annealed at 425°C under argon during 24 h. A third route (referred as R3) consisted in applying the spark plasma sintering (SPS) technique directly to a mixture of $TiS_2$, Ti and $Li_2S$ precursors in a graphite mold (all the precursors were introduced in the mold inside a glove-box).

*Preparation of thin film electrodes*: Lithium titanium sulfide thin films were prepared from these three different types of targets by radio-frequency magnetron sputtering, using an equipment (Plassys) connected to an argon-filled glove box. Before deposition, the sputtering chamber was evacuated to a background pressure of less than $6.10^{-7}$ Pa, then filled with high purity argon (99.9999%). Prior to each deposition, sputtering of a titanium target was performed on the shield to trap oxygen traces present in the chamber, then a pre-sputtering of the $LiTiS_2$ target was systematically carried out for 1 hour. All depositions were performed with no intentional heating/cooling of the substrate.

In order to compare the physicochemical and then the electrochemical properties of lithium titanium sulfide thin films prepared from the different $LiTiS_2$ targets, standard deposition conditions were defined as follows: pure argon as the discharge gas, a power of 1.27 W $cm^{-2}$, an argon flow of 20 $cm^3.min^{-1}$, a total pressure of 0.5 Pa and a target-substrate distance of 100 mm. These conditions were chosen to limit the incorporation of oxygen in the film and to facilitate the deposition of Li species. The latter are based on theoretical considerations, previous work dealing with the synthesis of $TiO_xS_y$ thin films from $TiS_2$ targets,[21] and of a preliminary study assessing the influence of the total pressure on the electrochemical behavior of the films synthesized from $LiTiS_2$ prepared by chemical reaction (see supplementary information Figure S1).

*Manufacture of all-solid-state microbatteries*: All-solid-state microbatteries having an active area of 7 or 25 $mm^2$ were manufactured by sequential deposition of thin films either on passivated 4'' silicon wafer (Siltronix) or on 4'' glass wafer (Schott) substrates. The typical active stack was W (250 nm)/ Li-Ti-S (0.5-1.0 μm)/LiPON (1.4 μm)/Li (3 μm), using the deposition conditions for W, LiPON and Li reported previously.[22] Photolithography was used to pattern the first level (W current collector); subsequent materials were deposited using shadow masking. At the end, wafers were capped with a polymer and a glass plate to protect the microbatteries from air and moisture.

*Physicochemical characterization of materials*: The chemical composition of Li-Ti-S thin films was determined by combining Rutherford backscattering spectroscopy (RBS) and Inductive coupled plasma (ICP) measurements (Table 1). RBS analysis was achieved at a backscattering angle of 150° using an incident beam of $4He^+$ ions with an energy of 2 MeV. The spectra were analyzed with the SIMNRA software.[23] For that purpose, 100 nm thick films were deposited onto vitreous carbon substrates. As lithium is not detected by RBS, the Li/Ti lithium content in the film was obtained using an inductively coupled plasma-optical emission spectrometer ICP-OES (Varian 720ES) using the following emission lines: $\lambda$ = 670.78 nm for Li, at $\lambda$ = 368.52 nm for Ti. Thin film samples deposited on the glass substrate were dissolved in 10 ml of HCl, then a small amount of the resulting solution was introduced in the spectrometer. The homogeneity of the film composition over the thickness was checked by Auger electron spectroscopy (VG Microlab 310 F) for samples deposited onto silicon wafers.

XPS measurements were carried out with a Thermo Scientific K-Alpha X-ray photoelectron spectrometer using a focused monochromatic Al Kα radiation (hν = 1486.6 eV) in order to determine the nature and the local environment of mainly Ti and S species. Besides, air-tight glass containers were systematically used to transfer thin film samples from the sputtering chamber to the glove-box

filled with purified argon and connected directly to the XPS spectrometer, in order to avoid the contamination of the surface. For the Ag $3d_{5/2}$ line the full width at half-maximum (FWHM) was 0.50 eV under the recording conditions. The X-ray spot size was 400 μm. Peaks were recorded with constant pass energy of 20 eV. The pressure in the analysis chamber was less than $2.10^{-8}$ Pa. Short acquisition time spectra were recorded at the beginning and at the end of each experiment to check that the samples did not suffer from degradation during the measurements. Peak assignments were made with respect to reference compounds analyzed in the same conditions. The binding energy scale was calibrated from the hydrocarbon contamination using the C 1s peak at 285.0 eV. Core peaks were analyzed using a nonlinear Shirley-type background.[24] Peak positions and areas were optimized by a weighted least-squares fitting method using 70% Gaussian and 30% Lorentzian line shapes. Quantification was performed on the basis of Scofield's relative sensitivity factors.[25] Analyses of lithiated/de-lithiated thin films were performed on electrode materials deposited on an aluminum foil and charged at 3.2 V/$Li^+$/Li or discharged at 1.5 V/$Li^+$/Li in button cells using a liquid electrolyte (EC:DMC 1:1, 1M $LiPF_6$, Novolyte). Mechanical erosion under ultrahigh vacuum was achieved before carrying out the analyses in order to remove the SEI (Solid Electrolyte Interphase) covering the surface of the thin-film electrode. This method is used instead of ionic bombardment because the latter is likely to induce a reduction of elements present in the electrode material.

X-ray diffraction was carried out with a Brucker D8 Advance diffractometer in Bragg-Bretano geometry using an air-tight cell filled with argon.

*Electrochemical characterization of materials*: Electrochemical measurements were performed using a VMP3 galvanostat-potentiostat (Bio-Logic) with channels equipped for electrochemical impedance spectroscopy (EIS) analysis. Preliminary electrochemical characterization of lithiated titanium sulfide thin films was carried out with a liquid electrolyte using 2032 button cells. These cells were assembled in a glove box under argon atmosphere using the thin film deposited on an aluminum disc

as the positive electrode, a polypropylene non-woven (Viledon FS2123, Freudenberg) and a microporous polypropylene film (Celgard 2400) as separators, a lithium foil (battery grade, Chemetall Foote) as the negative electrode and a liquid electrolyte 1M $LiPF_6$ in EC:DMC 1:1 (Novolyte). Aluminum substrates were weighted in the glove box before and after thin film deposition using a microbalance (0.1 µg accuracy).

All-solid-state microbatteries were electrically connected to the apparatus using shielded miniature probe heads (Cascade Microtech) and tungsten tips. Considering the microbattery design, measurements were performed using a two electrode set-up. Both the apparatus and microbatteries were kept at a controlled temperature of 25°C during measurements. The mass of electrode materials used in these microbatteries (~ 50 µg) were estimated *a priori* from the area of the pattern and the positive electrode thickness. Nevertheless, due to shadowing effects, the actual film thickness is actually lower at the edges of the pattern, hence the actual mass was systematically under-estimated. In order to determine more precisely the latter, a calibration was performed *a posteriori* on the basis of the specific capacity obtained for the first charge performed in button cells. The evolution of the open circuit voltage and the impedance of the microbatteries as a function of their state of charge (or the lithium content in the lithium titanium thin film electrode) were measured using the Galvanostatic Intermittent Titration Technique (GITT). The latter consisted in iterating sequences comprising a constant current pulse (2 µA $cm^{-2}$, ~5% capacity increment), followed by a 4 hours rest period and then by EIS measurements (voltage amplitude $\Delta E = \pm 10$ mV, frequency range 100 MHz -10 mHz).

## 3. Results and discussion

### 3.1. $LiTiS_2$ compounds and related sputtering targets

Sputtering targets of $LiTiS_2$ composition were synthesized via three distinct routes. The first one required the preparation of a $LiTiS_2$ powder by chemical lithiation of $TiS_2$ using n-butyl lithium (route R1). The characterization of the resulting product by X-Ray diffraction (Figure S2a) confirmed the synthesis of a pure 1T-$Li_xTiS_2$ phase, having the following refined hexagonal cell parameters a = b = 3.4501(2) Å, c= 6.1928(3) Å (P-3m1 space group). Therefore, the latter values confirm the full lithiation of the $TiS_2$ precursor and the achievement of the $LiTiS_2$ composition in agreement of the ICP analysis.[26] Besides, it was found that this $LiTiS_2$ powder retained the same plate-like shape of the pristine $TiS_2$ particles. As a consequence, the cold compaction carried on this anisotropic powder for shaping the target leads to a maximum compactness of only 61% (1.94 g $cm^{-3}$). Then, although $LiTiS_2$ is known to be thermally stable at least up to 800°C either under its 1T or 3R structural type,[20,27] additional conventional sintering aiming at increasing the compactness of the target was not conceivable due to the high chemical reactivity of the material.

An alternative route for the preparation of a $LiTiS_2$ target by solid state reaction of $TiS_2$, $Li_2S$ and Ti powdered precursors (route R2) was also investigated in the prospect for the preparation of larger targets. The course of the reaction was followed by *ex situ* XRD on pelletized samples annealed under argon during 20 hours between 400°C and 600°C. The corresponding diffraction patterns (Figure S2b) show the complete transformation of $TiS_2$ into a 1T-$LiTiS_2$ phase at 400°C, despite the presence of small amounts of unreacted Ti and $Li_2S$. Additional peaks, which correspond to the 3R-$Li_xTiS_2$ phase,[20] progressively grow when the temperature is further increased. At 600°C, the transformation of 1T-$LiTiS_2$ into 3R-$LiTiS_2$ is almost complete and is accompanied by the formation of a lithium titanium oxide impurity (likely $Li_4Ti_5O_{12}$). Finally, a thermal treatment of the target at 425°C during 40 hours was chosen as a trade-off to get the most complete reaction without the

formation of oxide impurities. The resulting density of the R2 target was estimated to ~1.60 g.cm$^{-3}$, which corresponds to a compactness of 52%. Finally, we had the opportunity to prepare a third target by spark plasma sintering using the same precursors. As expected, the rapid thermal annealing at 600°C of the $TiS_2$, Ti, $Li_2S$ blend then led to the preparation of a denser target (2.8 g cm$^{-3}$, i.e. ~ 91% compactness).

### 3.2. Physico-chemical properties of lithium titanium sulfide thin films

Lithium titanium sulfide thin film deposition using the same standard sputtering conditions (see experimental section) for each target leads to conventional deposition rates between 4.8 and 5.4 nm.min$^{-1}$, the highest one being achieved consistently with the denser target. SEM images (Figure S3) show that the resulting thin films exhibit a dense morphology and a very smooth surface that are well-adapted to the sequential process of manufacture of all-solid-state thin film batteries. All the films exhibit an amorphous character (XRD) and similar densities of 2.8 ± 0.1 g cm$^{-3}$. Chemical analyses by RBS and ICP-OES lead to the following film compositions (Table 1): $Li_{1.2}TiO_{0.5}S_{2.1}$ (target R1), $Li_{0.6}TiO_{0.6}S_{1.8}$ (target R2) and $Li_{1.0}TiO_{0.3}S_{2.0}$ (target R3). An example of RBS spectrum is given on Figure S4. The chemical homogeneity of these films was confirmed by Auger spectroscopy depth profiling. Therefore, as for thin films deposited by sputtering from a $TiS_2$ target,[21] it was found again that, despite all precautions taken to avoid oxygen contamination, a small oxygen amount is actually incorporated in the films. Titanium is indeed highly reactive even under high vacuum, a residual fraction of 0.7% of $O_2$ in the discharge gas being typically sufficient to fully oxidize Ti into $TiO_2$.[28] Nevertheless, since the amount of oxygen in the R3 film is only half of the oxygen content in the R2 film, it is clear that the density of the sputtering target influences also the oxygen incorporation in the film, a denser target leading to a lower oxygen content.

**Table 1.** Chemical composition of the $Li_xTiO_yS_z$ thin films deduced from ICP and RBS experiments

| Thin films | Li/Ti (ICP) | O/Ti (RBS) | S/Ti (RBS) | Chemical formula |
|---|---|---|---|---|
| R1 (Chemical lithiation) | 1.18 ±0.02 | 0.5 ±0.1 | 2.07 ±0.04 | $Li_{1.2}TiO_{0.5}S_{2.1}$ |
| R2 (Solid state reaction) | 0.62 ±0.02 | 0.6 ±0.1 | 1.80 ±0.04 | $Li_{0.6}TiO_{0.6}S_{1.8}$ |
| R3 (SPS of precursors) | 1.03 ±0.02 | 0.3 ±0.1 | 2.04 ±0.04 | $Li_{1.0}TiO_{0.3}S_{2.0}$ |

XPS analysis of the films deposited from the different targets was performed. The corresponding Ti2p and S2p spectra are shown in Figure 1. According to a previous study of $TiO_yS_z$ films,[21] $Ti2p_{3/2-1/2}$ core peaks for R1 films (Figure 1a) were fitted with three doublets: i) a doublet attributed to $Ti^{4+}$ ions in a sulfur environment as in $TiS_2$ (456.1 – 462.2 eV) or in $TiS_3$ (456.0 – 462.2 eV), ii) a doublet assigned to $Ti^{4+}$ ions in a majority oxygen environment considering the binding energy close to the reference for rutile $TiO_2$ (458.5 – 464.1 eV), iii) an additional doublet required to fit the experimental curve, located at intermediate binding energies between the two previous ones corresponding to titanium ions into a mixed oxygen-sulfur environment. Then, only $Ti^{4+}$ species were evidenced in the R1 sample, with relative amounts of 24%, 45% and 31%, respectively for $TiS_2$-$TiS_3$, TiOS and $TiO_2$-like environments (Table S1). The $S2p_{3/2-1/2}$ XPS core peak displays only one doublet at 161.0-162.2 eV assigned to $S^{2-}$ ions as in the $TiS_2$ reference compound (160.9 – 162.1 eV) or $TiS_3$ (161.0 – 162.1 eV).[21] These results are actually fully consistent with the charge balance for the $Li_{1.2}TiO_{0.5}S_{2.1}$ composition, and means that all the $Ti^{3+}$ present initially in the $LiTiS_2$ target is oxidized (by trapping oxygen traces) during the sputtering process.

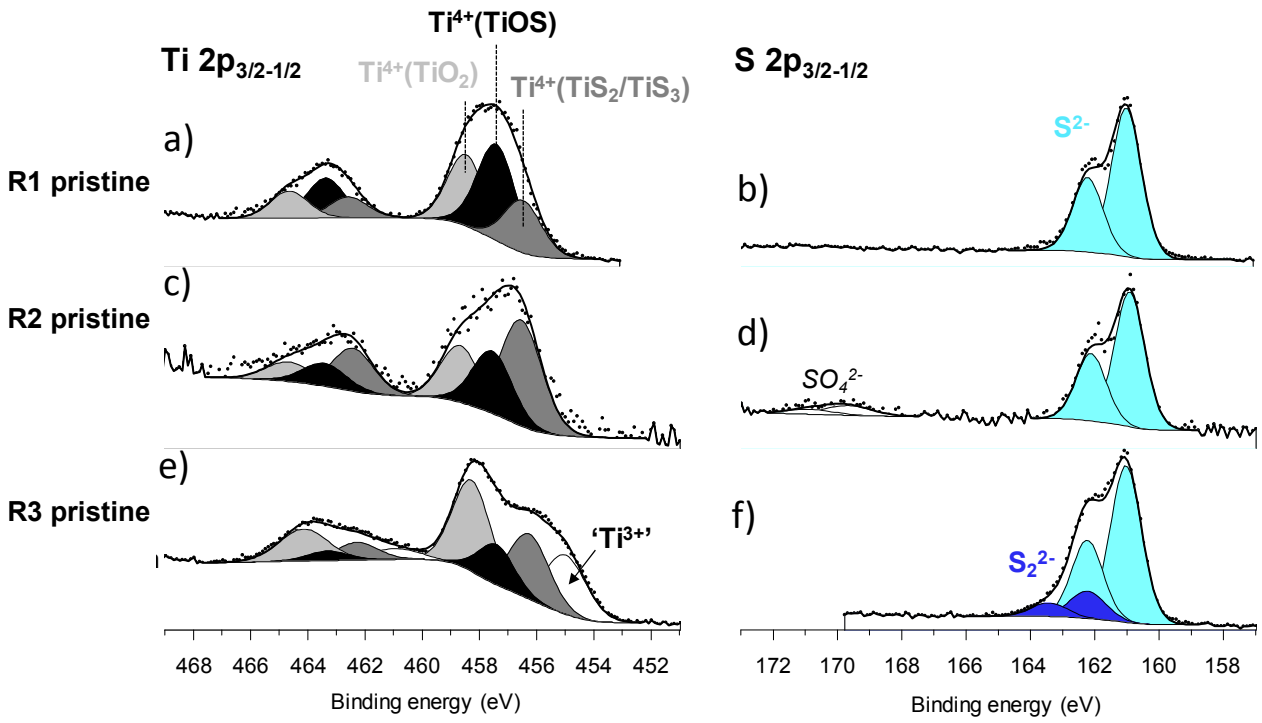


**Figure 1.** Ti 2p and S 2p core peak spectra of 'LiTiOS' thin films prepared from (a,b) R1, (c,d) R2 and (e,f) R3 targets using standard sputtering conditions.

The Ti2p spectrum of the R2 film exhibits the three same environments for titanium (Figure 1c) (sulfur, mixed oxygen-sulfur and oxygen environment) in relative amounts of 48%, 27% and 25% (Table S1). As for the R1 film, the $S2p_{3/2-1/2}$ spectrum (Figure 1b) clearly evidences the presence of only $S^{2-}$ ions. Note that a small component attributed to sulfate ions is detected at 169.7-170.9 eV, probably corresponding to contamination. As expected from the $Li_{0.6}TiO_{0.6}S_{1.8}$ film composition, XPS analysis is also consistent with a full $Ti^{4+}$ content. Consequently, as in $Li_{2-x}FeS_2$ materials,[29-31] further electrochemical lithium de-insertion from these electrodes should necessarily involve the oxidation of anionic species.

In the case of the R3 film, in addition to the doublets corresponding to $Ti^{4+}$ ions in the three types of environments ($TiS_2$-$TiS_3$ 25%, TiOS 14%, $TiO_2$ 38%), the $Ti2p_{3/2-1/2}$ XPS core peak (Figure 1e) exhibits a doublet located at 455.0-461.0 eV (23%) assigned to a more reduced state titanium species,

probably $Ti^{3+}$ ions. Moreover, the $S2p_{3/2-1/2}$ core peak (Figure 1f) displays a doublet at 161.0-162.2 eV corresponding to $S^{2-}$ ions (83%) and another one at 162.2-163.4 eV attributed to a small amount of sulfur in $S_2^{2-}$ disulfide pairs (17%). The relative percentages clearly reveal that the titanium in sulfur environment is closer to $TiS_2$ rather than $TiS_3$. Then, further redox processes accompanying the lithium de-insertion from this material should necessary involve both titanium and sulfur species.

### 3.3. Electrochemical behavior of Li-Ti-(O)S thin films – Sulfide anions participating to the redox process

The electrochemical behavior of the different $Li_xTiO_yS_z$ thin films was firstly assessed in liquid electrolyte cells. After assembly, the open circuit voltage of the series of cells prepared in standard conditions from R1, R2 and R3 targets was respectively 2.1, 2.2 and 1.6 V. Cyclic voltammetry (Figures 2a-c) was performed at first, starting by the oxidation (delithiation) of the material, in order to reveal the different electrochemical steps. The first oxidation of the films prepared with R1 and R2 targets proceeds with a single step at ~ 2.6 $V/Li^+/Li$, which is reversible (Figure 2a and Figure 2b). As the latter leads to the appearance of a new doublet on the S2p spectra (Figure 3) for both R1 and R2 electrodes, respectively located at 162.2-163.4 eV and 162.3-163.5 eV, which corresponds to $S_2^{2-}$ disulfide pairs, it can be clearly attributed to the oxidation of $S^{2-}$ in $S_2^{2-}$. Besides, quantitative analyses (Table S2) show that the $S_2^{2-}/S^{2-}$ ratio is higher in the fully oxidized R1 electrode than in the R2 one; this is consistent with the higher delithiation capacity theoretically expected from the initial film compositions ($Li_{1.2}TiO_{0.5}S_{2.1}$ for R1, $Li_{0.6}TiO_{0.6}S_{1.8}$ for R2) and also from the actual capacity measured during the first charge (Figure 2d). Compared to pristine materials, only a slight evolution of the $Ti2p_{3/2-1/2}$ core peaks occurs during the charge, the latter being connected to a small variation of the proportion of the three $Ti^{4+}$ environments.

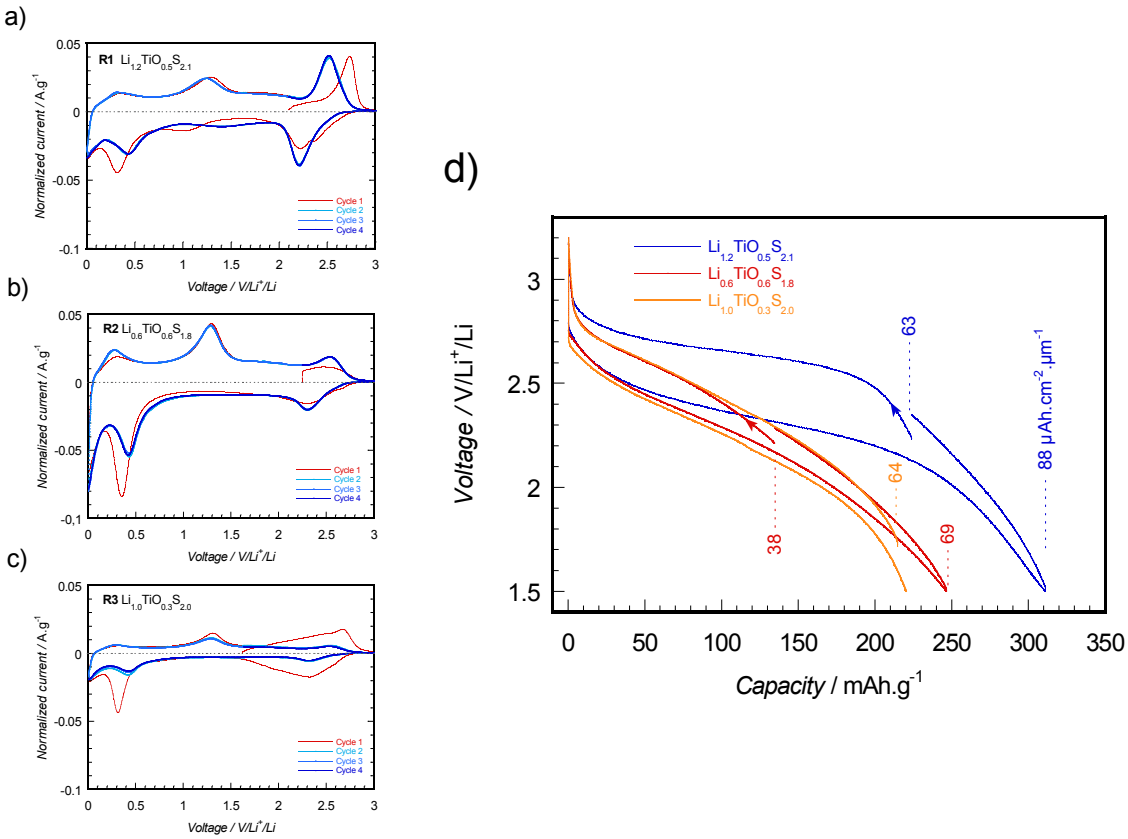


**Figure 2.** Electrochemical behavior of thin films in button cells (1M $LiPF_6$, EC:DMC 1:1 electrolyte). Cyclic voltammetry of thin film electrodes prepared from R1 (a), R2 (b) and R3 (c) targets (sweep rate 5 µV $s^{-1}$). Comparison of the first galvanostatic cycle (2 µA $cm^{-2}$) for the three materials (d), with indication of the volumetric capacity.

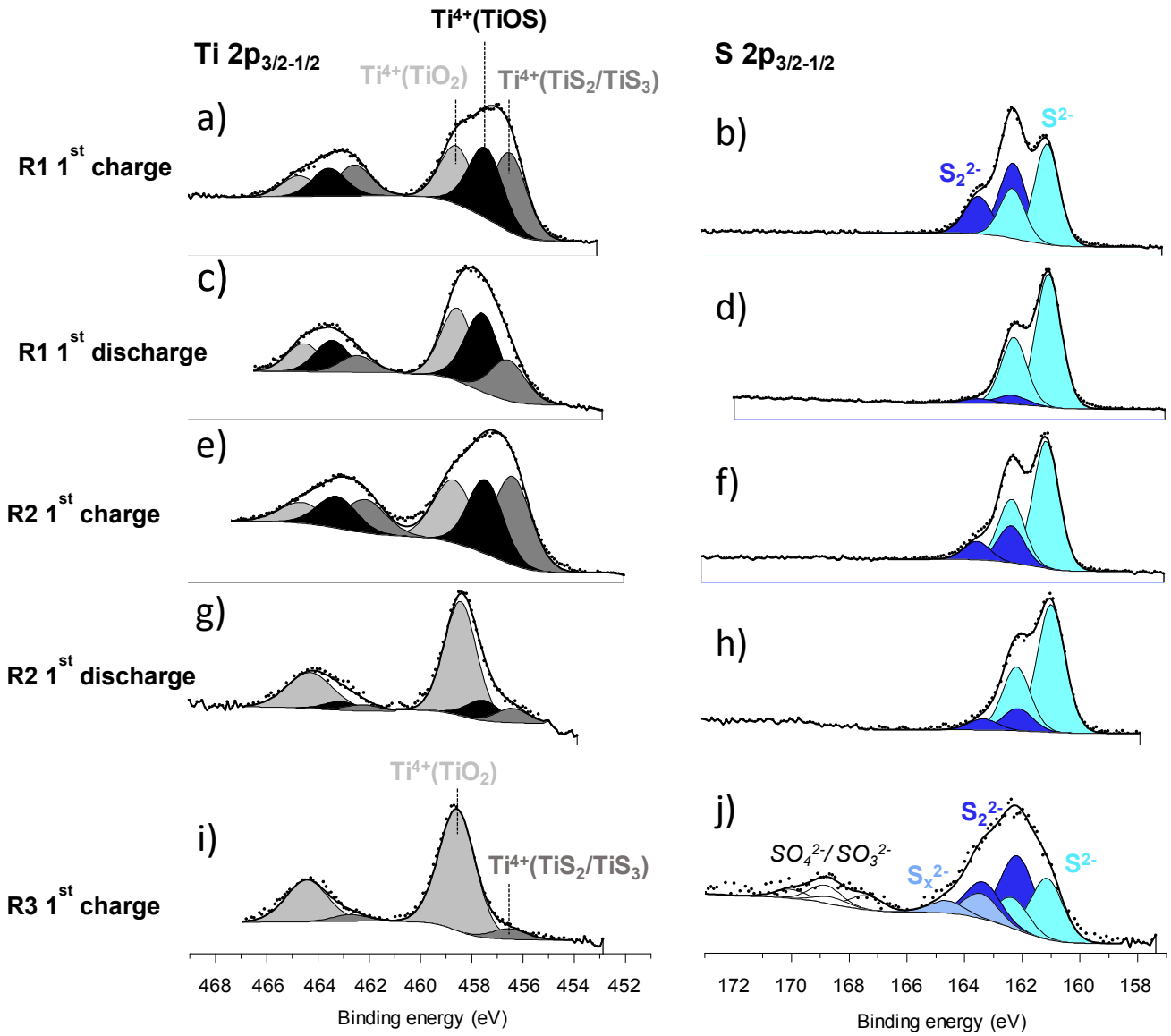


**Figure 3.** Evolution of Ti2p (a, c, e, g, i) and S2p (b, d, f, h, j) core peaks spectra between the end of the first charge at 3.2 V/$Li^+$/Li and the end of the subsequent discharge at 1.5 V/$Li^+$/Li, for the three types of films (R1, R2 and R3).

The first oxidation of the electrode prepared with the R3 target, starting from a significantly lower OCV, hence from a more reduced state compared to the two others, is characterized by a quite progressive increase of the current ending with a more marked peak at around 2.6 V/$Li^+$/Li attributable to the $S^{2-}/S_2^{2-}$ reaction (Figure 2c). Indeed, as deduced from the $S2p_{3/2-1/2}$ core peak

(Figure 3), it is also found here that the proportion of $S_2^{2-}$ species is significantly higher in the fully charged sample (40%) than in the pristine material (17%). Therefore, the first oxidation stages must be related to the oxidation of $Ti^{3+}$ initially present in the material into $Ti^{4+}$; then, titanium and sulfide-based processes partially overlap during the continuation of the oxidation and also during the subsequent reduction. Regarding the $Ti2p_{3/2-1/2}$ core peak spectrum, it reveals the disappearance of the '$Ti^{3+}$' doublet and presence of a majority of $TiO_2$-like environments (89%) that is quite surprising. The latter point and the increase of the '$TiO_2$' contribution in discharged R1 and R2 electrodes (Figure 3) suggest that extra '$TiO_2$' species are spontaneously formed when $Ti^{3+}$ species are in contact with the liquid electrolyte. The same reaction is likely to occur when the pristine R3 film is immersed in the liquid electrolyte, causing a spontaneous '$TiO_2$' enrichment at the surface that remains once the electrode is charged. Indeed, as it has been already evidenced for reduced $Li_4Ti_5O_{12}$ electrodes, $Ti^{3+}$ is prone to react with water traces and with ethylene carbonate.[32,33] Therefore, it is actually difficult to follow the course of the redox processes involving Ti species. Besides, a quite reversible process occurs also below 1.5 V (reduction peak at 0.4 V/$Li^+$/Li, then oxidation peak at 1.3 V/$Li^+$/Li) for all samples. The corresponding coulombic balance and other results related to the reduction of $TiS_2$ indicate that the latter corresponds to the $Ti^{3+}/Ti^{2+}$ redox reaction.[34,35]

The first galvanostatic cycle in the 1.5-3.2 V/$Li^+$/Li potential window is presented in Figure 2d for the three types of film. The voltage curve of the $Li_{1.2}TiO_{0.5}S_{2.1}$ film (R1 target) displays a long plateau at 2.6-2.7 V on which proceeds the extraction of almost all the lithium contained in the pristine material ($\Delta$xLi= -1.16) and the concomitant oxidation of $S^{2-}$ species. The full delithiation of $Li_{0.6}TiO_{0.6}S_{1.8}$ is also achieved during the first charge at 3.2 V. Nevertheless, whereas the same electrochemical process occurs, a lower polarization is measured here. Concerning the film from the R3 target, its voltage curve is quite identical to the one of $Li_{0.6}TiO_{0.6}S_{1.8}$, except that the starting point corresponds to a more reduced and lithiated material. Delithiation of this material proceeds with the oxidation of $Ti^{3+}$, then of $S^{2-}$ species, exhibiting a 40:60 capacity ratio, which is close to the

one expected from the initial $Li_{1.0}TiO_{0.3}S_{2.0}$ composition. The use of a denser '$LiTiS_2$' target actually allows enhancing the kinetics of erosion of the target surface at the expense of its oxygenation (poisoning) during the sputtering process, hence is a means of moving to a less reactive sputtering mode and preserving reduced titanium species.[36]

On the basis of the initial composition of the films and the charge balance, and assuming that $Ti^{3+}$ and $S_2^{2-}$ species do not coexist in the pristine materials, a formal distribution of the $Ti^{3+}/Ti^{4+}$ and $S^{2-}/S_2^{2-}$ redox processes involved during the first charge and the corresponding specific capacities can be proposed:

(R1) $Li_{1.2}Ti^{4+}O_{0.5}S^{2-}_{2.1} \rightarrow Ti^{4+}O_{0.5}S^{2-}_{0.9}S^{-}_{1.2} + 1.2\ Li^{+} + 1.2\ e^{-}$ *244 mAh g$^{-1}$*

(R2) $Li_{0.6}Ti^{4+}O_{0.6}S^{2-}_{1.6}S^{-}_{0.2} \rightarrow Ti^{4+}O_{0.5}S^{2-}_{0.9}S^{-}_{1.2} + 0.6\ Li^{+} + 0.6\ e^{-}$ *135 mAh g$^{-1}$*

(R3) $Li_{1.0}Ti^{4+}_{0.4}Ti^{3+}_{0.6}O_{0.3}S^{2-}_{2.0} \rightarrow Li_{0.4}Ti^{4+}O_{0.3}S^{2-}_{2.0} + 0.6\ Li^{+} + 0.6\ e^{-}$ ; $Li_{0.4}Ti^{4+}O_{0.3}S^{2-}_{2.0} \rightarrow Ti^{4+}O_{0.3}S^{2-}_{1.6}S^{-}_{0.4} + 0.4\ Li^{+} + 0.4\ e^{-}$ *217 (130 + 87) mAh g$^{-1}$*

These values are actually in good agreement with the experimental ones, both concerning the full charge capacity and the distribution of the cation- and anion-based redox processes in the R3 film.

Finally, first charge volumetric capacities of thin films prepared from R1 and R3 targets are quite identical (220 mAh $g^{-1}$ or 64 µAh $cm^{-2}$ $µm^{-1}$) and significantly higher than the one of the films prepared from the R2. They are close to the capacity reported for $LiCoO_2$ thin films.[13] As only this initial charge capacity can be actually used in a Li-ion system, additional electrochemical characterizations in solid state microbatteries were only performed on thin films having the highest capacities (i.e. R1 and R3 thin films). Moreover, these thin film electrodes illustrate respectively the case of electrode materials involving either the larger or the lower amount of sulfide species in the redox process.

All-solid-state Li/LiPON/$Li_xTiO_yS_z$ thin film batteries were then manufactured to study the electrochemical behavior of both $Li_xTiO_yS_z$ materials prepared from R1 and R3 targets (Figure 4). The stability of the voltage curves (shape and capacity value) versus cycles during constant current cycling in the 1.5 – 3.2 V/$Li^+$/Li range (Figure 5) highlights the perfect reversibility of the electrochemical processes in any case, whatever the current density. From both sample curves, it appears that the polarization is very low in the part of the curve involving the $Ti^{3+}/Ti^{4+}$ cation-based process, whereas it is greatly increased in the part involving mainly the $S^{2-}/S_2^{2-}$ anion-based process. This evolution is likely to originate from a marked decrease in the electronic conductivity in the material as the mixed-valence character of the material tends to disappear (i.e. full oxidation of $Ti^{3+}$ species). When increasing the current density up to 130 μA $cm^{-2}$ (~ 2C rate), the processes remain perfectly reversible in both materials. The slight increase of the polarization, visible along the main part of the charge/discharge curve, is mainly related to the ohmic drop in the LiPON electrolyte (~ 50 mV). Nevertheless, the polarization rises more significantly at the end of the charge, especially for the sample R1, inducing a slight decrease of the capacity for both materials. Then, this capacity is perfectly stable (-0.0015% / cycle) for hundreds of cycles.

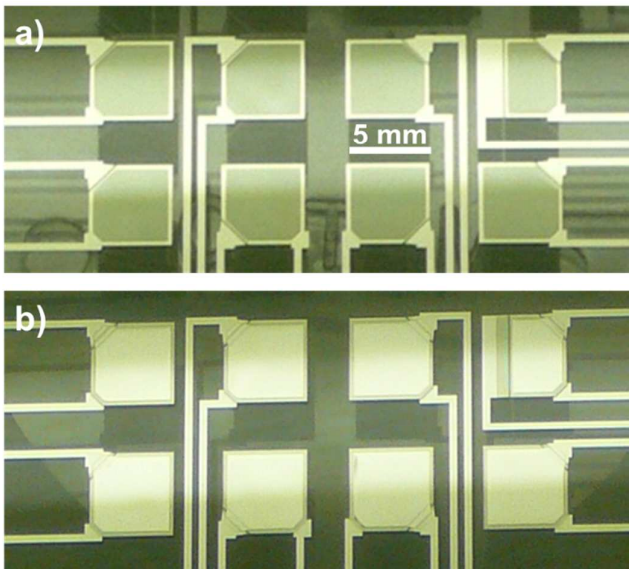


**Figure 4.** (a) W/LiTiOS thin film electrodes (25 $mm^2$) deposited on a glass substrate, prior to the deposition of the LiPON electrolyte and the lithium negative electrode. (b) Complete W/LiTiOS/LiPON/Li microbatteries.

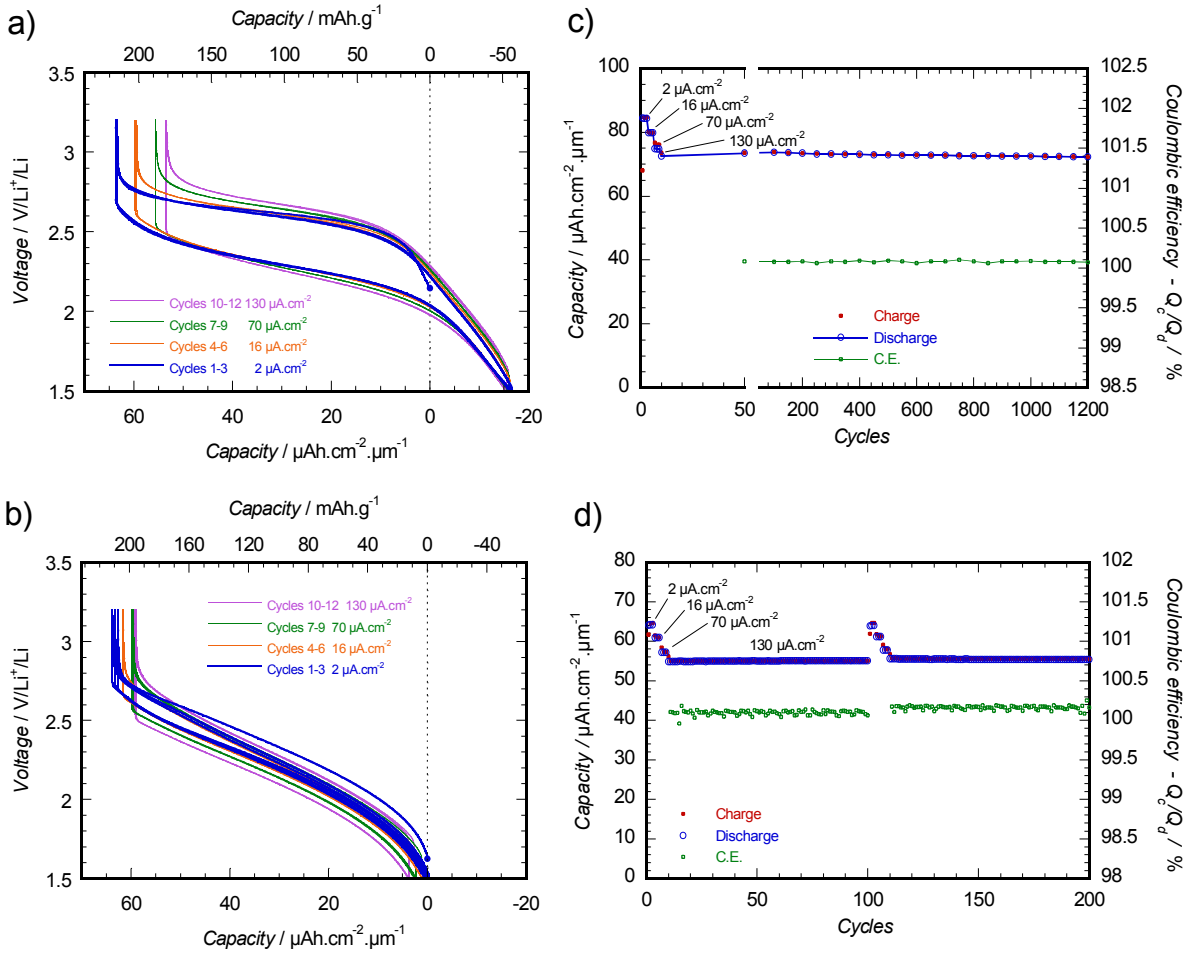


**Figure 5.** Galvanostatic cycling of (a) $Li_{1.2}TiO_{0.5}S_{2.1}$ (R1) and (b) $Li_{1.0}TiO_{0.3}S_{2.0}$ (R3) thin films in all-solid-state Li/LiPON/LiTiOS batteries at various current densities (130 µAh $cm^{-2}$ ~ 2C rate), and (c,d) the respective evolution of both their volumetric capacity and their coulombic efficiency. Insert shows W/$Li_{1.2}TiO_{0.5}S_{2.1}$ positive electrodes deposited on a glass wafer prior the achievement of the full all-solid-state cells.

The evolution of the impedance of a Li/LiPON/$Li_{1.2}TiO_{0.5}S_{2.1}$ (R1) microbattery was studied as a function of the state-of-charge (SOC) during a typical cycle between 1.5 V and 3.2 V (Figure 6), using a GITT protocol (Figure 7a). Between 0% and 90% SOC, the stable contribution of the LiPON electrolyte (first $R_{LiPON}$//$CPE_{LiPON}$ semi-circle) represents the major part of the impedance and only slight modifications of the medium-low frequency part related to the diffusion process and the charge

accumulation occur. Then, from 90% to 100% SOC, a new contribution appears and grows to become rapidly far larger than the electrolyte contribution. When discharging the cell, a reverse evolution is observed with the rapid fade of this additional contribution. Besides, as revealed in Figure 6a and Figure 6d, the characteristic frequency of the additional component is decreasing when the SOC is increasing (and *vice versa*).

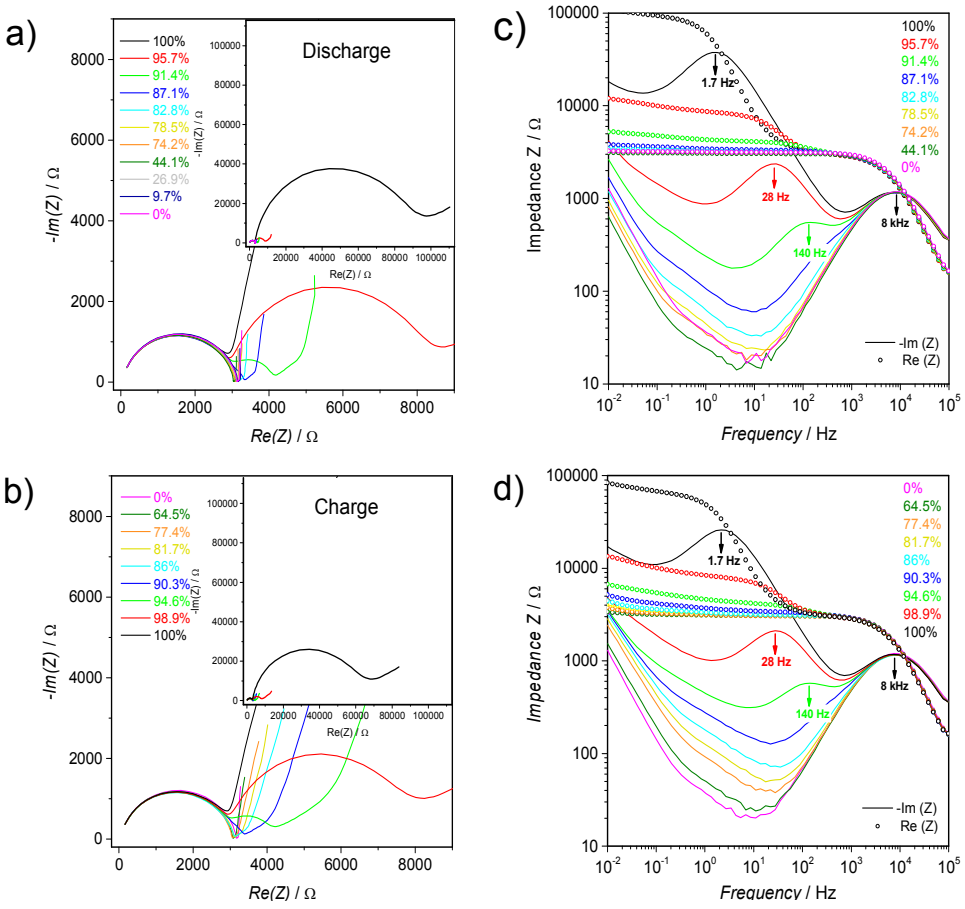


**Figure 6.** Two representations of the evolution of EIS spectra as a function of the state-of-charge of a Li/LiPON/ $Li_{1.2}TiO_{0.5}S_{2.1}$ (R1) microbattery during a discharge and the subsequent charge: (a,b) Nyquist diagrams and (c,d) the corresponding pseudo-Bode plots.

This contribution that could have been related to the formation of an interphase at the LiPON/$Li_xTiOS$ interface at the highest voltage values, is therefore more likely induced by a sharp increase of the charge transfer resistance at this interface when the electrode material is almost fully oxidized.[37] This is the phenomenon that actually hinders the complete delithiation of the material during charges carried out at high current rates (Figure 5a). A similar trend was also observed for Li/LiPON/LiTiOS (R3) cells.

In addition, calculation of the lithium diffusion coefficient ($\widetilde{D}_{Li^+}$) in $Li_xTiO_{0.5}S_{2.1}$ ($0 < x \leq 1.6$) materials was carried out by processing the Warburg part of these EIS spectra, using the method proposed by Huggins and *al.* and a fixed value of the molar volume ($V_M$) corresponding to 1T-$TiS_2$.[38] Thus, $\widetilde{D}_{Li^+}$ was found to increase regularly from $10^{-12}$ to $10^{-9}$ $cm^2.s^{-1}$ from the fully de-lithiated state to the $Li_{1.6}TiO_{0.5}S_{2.1}$ composition (Figure 7b). Examining these EIS results and other ones previously obtained for $TiO_{0.6}S_{1.6}$ sputtered films (i.e. containing ~ 0.2 $S_2^{2-}$ in the starting material),[18] it appears that in both cases a large decrease of $\widetilde{D}_{Li^+}$ (from $10^{-10}$ to $10^{-12}$ $cm^2$ $s^{-1}$ ) is observed concomitantly with the increase of the $S_2^{2-}$ pairs concentration. The shortening of some S-S distances (from 3.407-3.46 Å for $S^{2-}$ - $S^{2-}$ in $TiS_2$ to 2.04 Å for $(S\text{-}S)^{2-}$ in $TiS_3$ or amorphous $WS_3$ sulfides),[39-41] inducing a marked distortion of the anion network, is likely to be at the origin of this phenomenon. Finally, $\widetilde{D}_{Li^+}$ values measured in $Li_xTiO_{0.5}S_{2.1}$ materials are similar or slightly higher than the ones for $LiCoO_2$ and $LiMn_2O_4$ materials.[42-43]

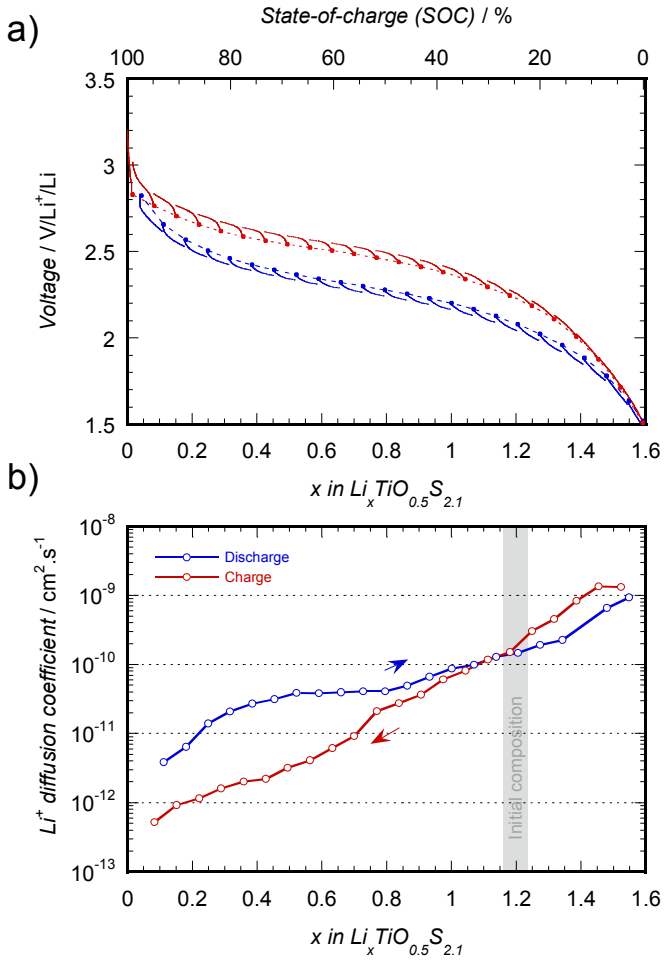


**Figure 7.** (a) Voltage profile of a Li/LiPON/ $Li_{1.2}TiO_{0.5}S_{2.1}$ (R1) microbattery measured during a GITT experiment. Dots correspond to the OCV measured after 4 hours of relaxation (blue: discharge, red: charge). EIS measurements were carried at the end of every rest period. (b) Lithium diffusion coefficient in $Li_xTiO_{0.5}S_{2.1}$ ($0 < x \leq 1.6$) calculated from EIS spectra.

Cross sections of all-solid-state Li/LiPON/$Li_{1.2}TiO_{0.5}S_{2.1}$ (R1) microbatteries prepared by Focus Ion Beam etching (Figure 8) were observed by SEM either in the charged or in the discharged state. They reveal a dense all-solid-state stack with well-defined interfaces, with no evidence of the formation of an eventual interphase between LiPON and the fully charged cathode. Besides, a noticeable volume change of the electrode (~ 20%) is generated between the charged and the

discharged states. The latter has obviously no detrimental effect on the cycling behavior of these microbatteries.

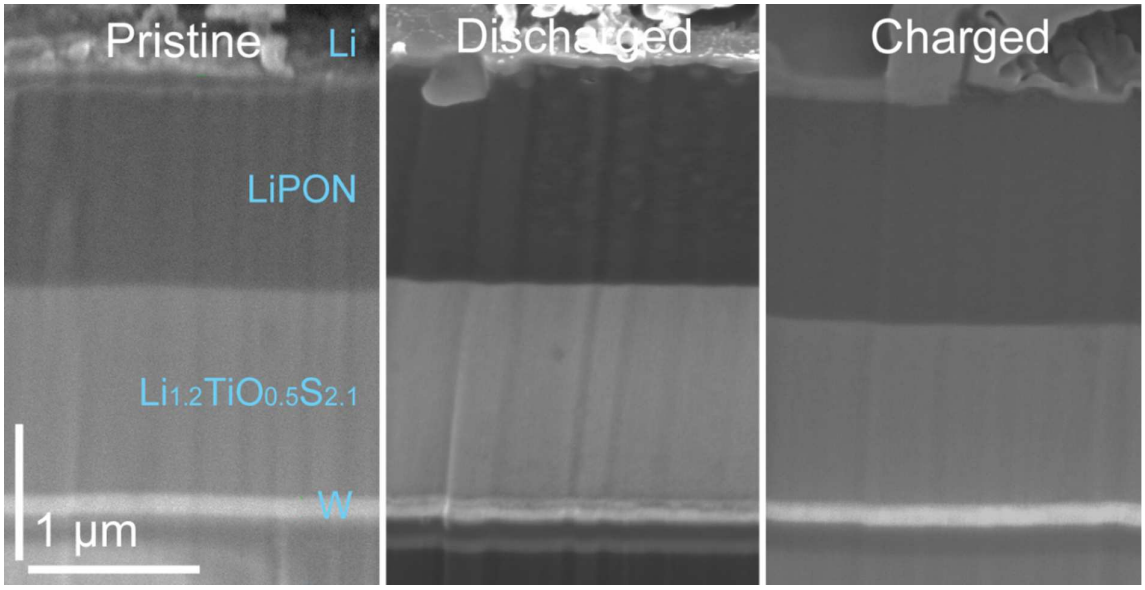


**Figure 8.** SEM-FIB image of Li/LiPON/$Li_{1.2}TiO_{0.5}S_{2.1}$ (R1) cells either in the pristine state, or stopped after hundreds of cycles either in the charged (3.2 V/$Li^+$/Li) and the discharged state (1.5 V/$Li^+$/Li).

## 4. Conclusion

Lithiated titanium oxysulphide thin film electrodes were prepared by sputtering from home-made targets having a $LiTiS_2$ composition. Target precursors, manufacturing process and the resulting compactness of the target were all found to clearly influence the composition of the films, hence their electrochemical behavior in all-solid-state microbatteries. Variations in the composition of the thin films are mainly related to the lithium content and the oxygen uptake during the sputtering process. While the first one directly influences the practical capacity of the electrode in a Li-ion system, the latter mainly determines the nature of the electrochemical processes occurring during the delithiation of these materials. Indeed, oxygen incorporation in the film proceeds with the oxidation

of Ti species originally present in the target into $Ti^{4+}$. As a consequence, it is observed a tendency to diverge from the $LiTiS_2$ targeted film composition towards $LiTiO_{0.5}S_2$. That initiates the participation of an increasing amount of anion species to the redox process ($S^{2-}/S_2^{2-}$ couple) at the expense of the $Ti^{3+}/Ti^{4+}$ process, inducing a progressive increase of both the mean operating voltage and the polarization. The use of targets having high compactness, as the ones prepared by SPS, is actually a promising means to achieve a better control of the process, hence of the composition of the films.

Finally, amorphous lithiated titanium oxysulphide thin film electrodes embedded in all-solid-state lithium microbatteries were able to deliver capacities as high as 85 µAh $cm^{-2}$ $µm^{-1}$ (or 270 mAh $g^{-1}$), of which a useful part of 65 µAh $cm^{-2}$ $µm^{-1}$, i.e. the same as for $LiCoO_2$, is actually usable in the prospect of an integration in a Li-ion cell.[11] Operation involving cation and/or anion-based redox processes revealed in any case the perfect reversibility of the latter and an excellent capacity retention (-0.0015% $cycle^{-1}$) during several hundreds of cycles. Contrary to $LiCoO_2$, the synthesis of these high capacity lithiated thin film electrodes does not require any annealing nor careful control of the preferred crystal orientation,[13,44,45] hence is simple and is interestingly compatible with the deposition on flexible polymer substrates. Finally, taking into account the facile oxidation of $Ti^{3+}$ during the sputtering process and the perfect reversibility of the anion-based redox process, the preparation of thin electrodes from $Li_2S$-$TiS_2$ target compositions appears as a promising prospect.[46]

## Supporting Information

Electrochemical behavior of R1 ‘LiTiOS’ films prepared with different total pressures, XRD patterns of $LiTiS_2$ powders prepared by chemical lithiation of $TiS_2$ (R1) and by solid state reaction of $2Li_2S$:Ti:$3TiS_2$ (R2 and R3 target), SEM images of R1 and R2 thin films, RBS analysis of the R1 thin film and quantitative XPS analyses of ‘LiTiOS’ thin films performed before and after electrochemical cycling.

## Acknowledgements

This work was partly supported by the French Ministry of industry and STMicroelectronics in the framework of the Investissements d'Avenir program (Tours2015 project). Jean-Marc Boissel (CEA) is acknowledged for having completed the manufacture of microbatteries at CEA Grenoble. The authors are also grateful to Stéphanie Sorieul from the AIFIRA platform (CENBG-CNRS/IN2P3 - Bordeaux University) for her help in acquiring RBS spectra and Michel Lahaye (ICMCB) for Auger Electron Spectroscopy depth profiling.

## References

(1) MacKenzie, J. D.; Ho, C. Perspectives on Energy Storage for Flexible Electronic Systems. *Proc. IEEE* **2015**, *103*, 535-553.

(2) Wang, Y.; Liu, B.; Li, Q.; Cartmell, S.; Ferrara, S.; Deng, Z. D.; Xiao, J. Lithium and Lithium-ion Batteries for Applications in Microelectronic Devices: A Review. *J. Power Sources* **2015**, *286*, 330.

(3) Cymbet Home Page: http://www.cymbet.com (accessed Dec 15, 2016).

(4) Front Edge Technology Home Page: http://www.frontedgetechnology.com (accessed Dec 15, 2016).

(5) Prologium Home Page: http://www.prologium.com (accessed Dec 15, 2016).

(6) ST Microelectronics EFL700 Datasheet: http://www.st.com/content/st_com/en/products/power-management/battery-management-ics/enfilm-thin-film-batteries/efl700a39.html (accessed Dec 15, 2016).

(7) Kanehori, K.; Matsumoto, K.; Miyauchi, K.; Kudo, T. Thin Film Solid Electrolyte and its Application to Secondary Lithium Cell. *Solid State Ionics* **1983**, *9-10*, 1445-1448.

(8) Jourdaine, L.; Souquet, J. L.; Delord, V.; Ribes, M. Lithium Solid State Glass-based Microgenerators. *Solid State Ionics* **1988**, *20-30*, 1490-1494.

(9) Meunier, G.; Dormoy, R.; Levasseur, A. New Positive Electrode Materials for Lithium Thin Film Secondary Batteries. *Mater. Sci. Eng. B* **1989**, *83*, 19-23.

(10) Bates, J. B.; Dudney, N. J.; Gruzalski, G. R.; Zuhr, R. A.; Choudhury, A.; Luck, C. F.; Robertson, J. D. Fabrication and Characterization of Amorphous Lithium Electrolyte Thin Films and Rechargeable Thin-film Batteries. *J. Power Sources*, **1993**, *43*, 103-110.

(11) Le Cras, F.; Pecquenard, B.; Dubois, V.; Phan, V. P.; Guy-Bouyssou, D. All-solid-state Lithium-ion Microbatteries using Silicon Nanofilm Anodes: High Performance and Memory Effect. *Adv. Energy Mater.* **2015**, *5*, 1501061.

(12) Neudecker, B. J.; Dudney, N. J.; Bates, J. B. "Lithium-free" Thin-film Battery with In Situ Plated Li Anode. *J. Electrochem. Soc.* **2000**, *147*, 517-523.

(13) Bates, J. B.; Dudney, N. J.; Neudecker, B. J.; Hart, F. X.; Jun, H. P.; Hackney, S. A. Preferred Orientation of Polycrystalline $LiCoO_2$ Films. *J. Electrochem. Soc.* **2000**, *147*, 59-70.

(14) Dudney, N. J.; Jang, Y. I. Analysis of Thin-film Lithium Batteries with Cathodes of 50 nm to 4 μm Thick $LiCoO_2$. *J. Power Sources* **2003**, *119-121*, 300-304.

(15) Liao, C. L.; Fung, K. Z. Lithium Cobalt Oxide Cathode Film Prepared by RF Sputtering. *J. Power Sources* **2004**, *128*, 263-269.

(16) Park, H. Y.; Nam, S. C.; Lim, Y. C.; Choi, K. G.; Lee, K. C.; Park, G. B.; Kim, J. B.; Kim, H. P.; Cho, S. B. $LiCoO_2$ Thin Film Cathode Fabrication by Rapid Thermal Annealing for Micro Power Sources. *Electrochimica Acta* **2007**, *52*, 2062-2067.

(17) Shiraki, S.; Oki, H.; Takagi, Y.; Suzuki, T.; Kumatani, A.; Shimizu, R.; Haruta, M.; Ohsawa, T.; Sato, Y.; Ikuhara, Y.; Hitosugi, T. Fabrication of All-solid-state Battery using Epitaxial $LiCoO_2$ Thin Films. *J. Power Sources* **2014**, *267*, 881-887.

(18) Fleutot, B.; Pecquenard, B. ; Le Cras, F.; Delis, B.; Martinez, H.; Dupont, L.; Guy-Bouyssou, D. Characterization of All-solid-state Li/LiPONB/TiOS Microbatteries Produced at the Pilot Scale. *J. Power Sources* **2011**, *196*, 10289-10296.

(19) Dines, M. B. Lithium Intercalation via n-butylithium of the Layered Transition Metal Dichalcogenides. *Mater. Res. Bull.* **1975**, *10*, 287-292.

(20) Wiedemann, D.; Nakhal, S.; Senyshyn, A.; Bredow, T.; Lerch, M. The High-temperature Transformation from 1T- to 3R-$Li_xTiS_2$ (x = 0.7, 0.9) as Observed In Situ with Neutron Powder Diffraction. *Z. Phys. Chem.* **2015**, *229*, 1275-1288.

(21) Lindic, M. H.; Pecquenard, B.; Vinatier, P.; Levasseur, A.; Martinez, H. ; Gonbeau, D.; Petit, P. E.; Ouvrard, G. Characterization of RF Sputtered $TiO_yS_z$ Thin Films. *Thin Solid Films* **2005**, *484*, 113-123.

(22) Phan, V. P.; Pecquenard, B.; Le Cras, F. High-performance All-solid-state Cells Fabricated with Silicon Electrodes. *Adv. Funct. Mater.* **2012**, *22*, 2580-2584.

(23) Eckstein, W.; Mayer, M. Rutherford Backscattering from Layered Structures Beyond the Single Scattering Model. *Nucl. Instrum. Methods Phys. Res., Sect. B* **1999**, *153*, 337-344.

(24) Shirley, D. A. High-resolution X-ray Photoemission Spectrum of the Valence Bands of Gold. *Phys. Rev. B* **1972**, *5*, 4709.

(25) Scofield, J. H. Photoionization Cross Sections at 1254 and 1487 eV. *J. Electron. Spectrosc*. **1976**, *8*, 129-137.

(26) Whittingham, M. S. The Role of Ternary Phases in Cathode Reactions. *J. Electrochem. Soc*. **1976**, *123*, 315-320.

(27) Colbow, J.; Dahn, J. R.; Haering, R. R. The 3R Phase of $Li_xTiS_2$. *J. Power Sources* **1989**, *26*, 301-307.

(28) Donaghey, L. F.; Geraghty, K. G. Effect of Target Oxidation on Reactive Sputtering Rates of Titanium in Argon-Oxygen Plasmas. *Thin Solid Films* **1976**, *38*, 271-280.

(29) Blandeau, L.; Ouvrard, G.; Calage, Y.; Brec, R.; Rouxel, J. Transition-metal Dichalcogenides from Disintercalation Processes. Crystal Structure Determination and Mössbauer Study of $Li_2FeS_2$ and its Disintercalates $Li_xFeS_2$ ($0.2 \leq x \leq 2$). *J. Phys. C: Solid State Phys.* **1987**, *20*, 4271-4281.

(30) Barker, J.; Kendrick, E. The Electrochemical Insertion and Safety Properties of the Low-cost Li-ion Active Material, $Li_2FeS_2$. *J. Power Sources* **2011**, *196*, 6960-6963.

(31) Pelé, V.; Flamary, F.; Bourgeois, L.; Pecquenard, B.; Le Cras, F. Perfect Reversibility of the Lithium Insertion in $FeS_2$: The Combined Effects of All-solid-state and Thin Film Cell Configurations. *Electrochem. Comm.* **2015**, *51*, 81-84.

(32) Lu, X.; Gu, L.; Hu, Y. S.; Chiu, H. C.; Li, H.; Demopoulos, G. P.; Chen, L. New Insight into the Atomic-scale Bulk and Surface Structure Evolution of $Li_4Ti_5O_{12}$ Anode. *J. Am. Chem. Soc.* **2015**, *137*, 1581-1586.

(33) He, M.; Castel, E.; Laumann, A.; Nuspl, G.; Novák, P.; Berg, E. J. In Situ Gas Analysis of $Li_4Ti_5O_{12}$ Based Electrodes at Elevated Temperatures. *J. Electrochem. Soc.* **2015**, *162*, A870-A876.

(34) Murphy, D. W.; Carides, J. N. Low Voltage Behavior of Lithium/Metal Dichalcogenide Topochemical Cells. *J. Electrochem. Soc.* **1979**, *126*, 349-351.

(35) Kim, Y.; Park, K.; Song, S. H.; Han, J.; Goodenough, J. B. Access to $M^{3+}/M^{2+}$ Redox Couples in Layered $LiMS_2$ Sulfides ($M = Ti, V, Cr$) as Anodes for Li-ion Battery. *J. Electrochem. Soc.* **2009**, *156*, A703-A708.

(36) Schiller, S.; Beister, G.; Sieber, W. Reactive High Rate D.C. Sputtering: Deposition Rate, Stoichiometry and Features of $TiO_x$ and $TiN_x$ Films with Respect to the Target Mode. *Thin Solid Films* **1984**, *111*, 259-268.

(37) Iriyama, Y.; Kako, T.; Yada, C.; Abe, T.; Ogumi, K. Charge Transfer Reaction at the Lithium Phosphorus Oxynitride Glass Electrolyte/Lithium Cobalt Oxide Thin Film Interface. *Solid State Ionics* **2005**, *176*, 2371-2376.

(38) Ho, C.; Raistrick, I. D.; Huggins, R. A. Application of A-C Techniques to the Study of Lithium Diffusion in Tungsten Trioxide Thin Films. *J. Electrochem. Soc.* **1980**, *127*, 343-350.

(39) Chianelli, R. R.; Scanlon, J. C.; Thompson, A. H. Structure Refinement of Stoichiometric $TiS_2$. *Mater. Res. Bull.* **1975**, *10*, 1379-1382.

(40) Fureseth, S.; Brattås, L.; Kjekshus, A. On the Crystal Structures of $TiS_3$, $ZrS_3$, $ZrSe_3$, $ZrTe_3$, $HfS_3$ and $HfSe_3$. *Acta Chem. Scand., Ser. A* **1975**, *29*, 623-631.

(41) Hibble, S. J.; Walton, R. I.; Feaviour, M. R.; Smith, A. D. Sulfur–Sulfur Bonding in the Amorphous Sulfides $WS_3$, $WS_5$, and $Re_2S_7$ from sulfur K-edge EXAFS studies. *J. Chem. Soc., Dalton Trans.* **1999**, *16*, 2877-2883.

(42) Xia, H.; Lu, L.; Ceder, G. Li Diffusion in $LiCoO_2$ Thin Films Prepared by Pulsed Laser Deposition. *J. Power Sources* **2006**, *159*, 1422-1427.

(43) Xie, J.; Tanaka, T.; Imanishi, N.; Matsumura, T.; Hirano, A.; Takeda, Y.; Yamamoto, O. Li-ion Transport Kinetics in $LiMn_2O_4$ Thin Films Prepared by Radio Frequency Magnetron Sputtering. *J. Power Sources* **2008**, *180*, 576-581.

(44) Bouwman, P. J.; Boukamp, B. A.; Bouwmeester, H. J. M.; Wondergem, H. J.; Notten, P. H. L. Structural Analysis of Submicrometer $LiCoO_2$ Films *J. Electrochem. Soc.* **2001**, *148*, A311-A317.

(45) Yoon, Y.; Park, C.; Kim, J.; Shin, D. Lattice Orientation Control of Lithium Cobalt Oxide Cathode Film for All-solid-state Thin Film Batteries. *J. Power Sources* **2013**, *226*, 186-190.

(46) Sakuda, A.; Takeuchi, T.; Okamura, K.; Kobayashi, H.; Sakaebe, H.; Tatsumi, K.; Ogumi, Z. Rock-salt-type Lithium Metal Sulphides as Novel Positive-electrode Materials. *Sci. Rep.* **2014**, *4*, 4883.

## TOC/Abstract Graphic